PCCP

Electronic-Vibrational Density Evolution in a Perylene Bisimide Dimer: Mechanistic Insights into Excitation Energy Transfer

SCHOLARONE™
Manuscripts

Electronic-Vibrational Density Evolution in a Perylene Bisimide Dimer: Mechanistic Insights into Excitation Energy Transfer

Sohang Kundu[1] and Nancy Makri[1,2,*]

[1]Department of Chemistry, University of Illinois, Urbana, Illinois 61801
[2]Department of Physics, University of Illinois, Urbana, Illinois 61801
[*]Corresponding author. Email: nmakri@illinois.edu

Abstract

The process of excitation energy transfer (EET) in molecular aggregates is etched with the signatures of a multitude of electronic and vibrational time scales that often are extremely difficult to resolve. The effect of the motion associated with one molecular vibration on that of another is fundamental to the dynamics of EET. In this paper we present simple theoretical ideas along with fully quantum mechanical calculations to develop a comprehensive mechanistic picture of EET in terms of the time evolution of electronic-vibrational densities (EVD) in a perylene bisimide (PBI) dimer, where 28 intramolecular normal modes couple to the ground and excited electronic states of each molecule. The EVD motion exhibits a plethora of dynamical features, which impart physical justification for the composite effects observed in the EET dynamics. Weakly coupled vibrations lead to classical-like motion of the EVD center on each electronic state, while highly nontrivial EVD characteristics develop under moderate or strong exciton-vibration interaction, leading to the formation of split or crescent-shaped densities, as well as density retention that slows down energy transfer and creates new peaks in the electronic populations. Pronounced correlation effects are observed in two-mode projections of the EVD, as a consequence of indirect vibrational coupling between uncoupled normal modes induced by the electronic coupling. Such indirect coupling depends on the strength of exciton-vibration interactions as well as the frequency mismatch between the two modes and leaves nontrivial signatures in the electronic population dynamics. The collective effects of many vibrational modes cause a partial smearing of these features through dephasing.

I. Introduction

A detailed mechanistic picture of the dynamics that follows electronic excitation of molecular aggregates is highly desirable for a comprehensive understanding of excitation energy transfer (EET).[1] Physically motivated analyses of the spatiotemporal evolution of electronic-vibrational (EV) probability densities on electronic potential surfaces are essential for the assignment of features in the population dynamics, the interpretation of two-dimensional time-resolved spectra and the design of energy-efficient materials. A significant majority of theoretical approaches to simulate EET in the past have focused on the purely electronic reduced density matrix (RDM), which involves a trace with respect to the vibrational degrees of freedom. While the electronic populations and coherences are often the relevant quantities for describing the distribution of energy flow in molecular aggregates, the intricate interplays of vibrational density evolution, which underlies the specifics of RDM dynamics, remain hidden under the trace.

Recent theoretical treatments have explicitly incorporated one or a few vibrational degrees of freedom within the target subsystem, leading to several vibronic models, while the remaining vibrational modes were either neglected or delegated to a different level of treatment, e.g. as a dissipative continuous bath that is coupled to the electronic states and/or the special "system" mode. Unless substantiated by accurate electronic structure calculations for specific systems, such designations of a special mode within the broad and general framework of EET tend to be *ad hoc*. Moreover, many of these approaches have used a two-state approximation for the special mode, and/or relied on dynamical assumptions for the treatment of exciton-vibration coupling and/or the inclusion of finite temperature effects.[2-5]

In this paper we seek to obtain a detailed and thorough understanding of EET driven by the following fundamental questions: (i) How does the motion associated with a vibrational mode of a molecule modulate the dynamics of energy transfer to and from the molecule? (ii) What is the dynamical effect of one vibrational mode on another mode of the same or a neighboring molecule? (iii) How does the overall dynamics change when many vibrational modes of non-commensurate frequencies and couplings are simultaneously involved?

We provide answers to these questions by examining the time evolution of the probability density created along chosen vibrational coordinates by electronic excitation and intermolecular energy transfer in a Frenkel exciton-coupled homodimer of PBI-1, a bay-substituted perylene bisimide dye,[6, 7] which exhibits most of the typical effects of exciton-vibration dynamics. The J-aggregates of this molecule have received much attention because of their high fluorescence quantum yield.[8-10] We assume that the energy is initially localized in one the two monomers, following a Franck-Condon excitation from the ground state. Such a localized state is the superposition of the two delocalized exciton eigenstates that are commonly excited with an ultrafast laser pulse. We obtain highly accurate results by explicitly treating *all* vibrations at a fully quantum mechanical level within the Hamiltonian at room temperature, without invoking dynamical approximations or assumptions. The outcome of this investigation is an intricate analysis of EV motion on the molecular potential surfaces and its signatures in the observed electronic population dynamics, which reveals the complexity of the nonadiabatic dynamics in reduced-dimension two-mode models of the dimer, as well as the cumulative effects on this dynamics from the remaining intramolecular vibrations.

We begin with a basic analysis of EV dynamics in a dimer, which provides the theoretical framework for understanding the behaviors revealed by our numerical results. In section II we describe the Hamiltonian, which involves two electronic states and 28 intramolecular normal mode vibrations in each

molecular unit, along with Frenkel exciton interactions between the two molecules. We define two-mode electronic-vibrational densities (EVD), where either a particular mode on each of the monomers or two distinct modes on the same molecule are probed, either in isolation or in the presence of all remaining intramolecular modes. In section III we present some general theoretical considerations regarding the main factors that govern the EVD evolution in the dimer. In spite of its simplicity, this analysis highlights some of the important differences and subtle physical features that dictate the motion of vibrational modes that belong to a single molecule or to the two molecular units. Guided by these ideas, the time scales of electronic and vibrational degrees of freedom in PBI-1, and our earlier observations,[11, 12] we give at the beginning of section IV a summary of the main EV effects that underlie the electronic population dynamics in the PBI-1 dimer.

The results of our numerical calculations are presented in section IV. In the first part of this section we address the question posed in (i) by showing images of the obtained two-mode EVD for the PBI-1 dimer at select times, for a single vibrational mode in each molecule whose frequency is lower or higher than the frequency associated with the electronic transfer, and also for the near-resonant vibronic mode that is characterized by a relatively large Huang-Rhys factor. The EVD evolution provides visual justification for the key features of exciton-vibration dynamics identified in section III. Next, we address question (ii) by examining the EV motion of two different vibrational modes within the same molecule. Signatures of indirect vibrational coupling of uncoupled normal modes are identified for different combinations of vibrations. Finally, in the last part of that section we turn to question (iii) and investigate the collective effects from all molecular vibrations on the EVD evolution. All our density snapshots are supplemented with full animations in the Supporting Information. A summary and some concluding remarks are given in section V.

II. Hamiltonian, observables and methods

Consider a dimer of two identical molecules A and B, each being treated as a pair of ground and excited electronic states denoted by 0 and 1 respectively. The electronic Hamiltonian H_{el} relevant to EET comprises two states, $|1_A 0_B\rangle$ and $|0_A 1_B\rangle$, which couple through a Frenkel exciton term[13] with coupling parameter J,

$$\hat{H}_{el} = -J\left(|1_A 0_B\rangle\langle 0_A 1_B| + |0_A 1_B\rangle\langle 1_A 0_B|\right). \tag{2.3}$$

Each molecule also includes its own set of discrete intramolecular vibrations. We express the exciton-vibration coupling of vibrational normal mode i on monomer α to its ground and excited electronic states using unshifted and shifted harmonic oscillator terms,

$$\hat{h}_{i\alpha}^0 = \left(\frac{\hat{p}_{i\alpha}^2}{2m} + \frac{1}{2}m\omega_i^2 \hat{q}_{i\alpha}^2\right)|0_\alpha\rangle\langle 0_\alpha|, \ \hat{h}_{i\alpha}^1 = \left(\frac{\hat{p}_{i\alpha}^2}{2m} + \frac{1}{2}m\omega_{i\alpha}^2\left(\hat{q}_{i\alpha} - \frac{c_{i\alpha}}{m\omega_i^2}\right)^2\right)|1_\alpha\rangle\langle 1_\alpha|, \tag{2.4}$$

where α is either A or B, $p_{i\alpha}$ and $q_{i\alpha}$ are the mass-weighted ($m = 1$) momenta and coordinates, while $\omega_{i\alpha}$ and $c_{i\alpha}$ denote the respective vibrational frequencies and exciton-vibration coupling parameters. The displacement $q_{i\alpha}^{min} = c_{i\alpha}/m\omega_{i\alpha}^2$ characterizes the shift between the minima of the ground and excited state

3

potential energy surfaces along mode i due to exciton-vibration coupling and are often obtained from measured Huang-Rhys factors.[14] The overall Hamiltonian matrix for the dimer, written in the basis of the $|1_A 0_B\rangle$ and $|0_A 1_B\rangle$ states, is

$$\hat{H}_{\text{dimer}}^{\nu_A \nu_B} = \begin{pmatrix} \sum_{i=1}^{\nu_A} \hat{h}_{iA}^1 + \sum_{i=1}^{\nu_B} \hat{h}_{iB}^0 & -J \\ -J & \sum_{i=1}^{\nu_A} \hat{h}_{iA}^0 + \sum_{i=1}^{\nu_B} \hat{h}_{iB}^1 \end{pmatrix} \tag{2.5}$$

where ν_A and ν_B denote the included number of vibrational normal modes of molecules A and B. In the case of PBI-1, our full-space calculations include $\nu_A = \nu_B = 28$ vibrational modes with parameters obtained by Kühn and coworkers[15] using time-dependent density functional theory. We use the exciton coupling value $J = 514 \text{ cm}^{-1}$ obtained from the same work. However, we also consider the evolution of observables obtained with smaller numbers of vibrational modes, in order to distinguish the effects of different modes on the dynamics.

We assume that at $t = 0$ monomer A undergoes a "vertical" Frank-Condon (FC) electronic excitation, which leaves the intramolecular vibrations of both molecules still equilibrated to their respective ground electronic states. The initial density matrix is given by

$$\hat{\rho}_{\text{dimer}}^{\nu_A \nu_B}(0) = |1_A 0_B\rangle\langle 1_A 0_B| \prod_{i=1}^{\nu_A} \frac{e^{-\beta \hat{h}_{iA}^0}}{\text{Tr } e^{-\beta \hat{h}_{iA}^0}} \prod_{i=1}^{\nu_B} \frac{e^{-\beta \hat{h}_{iB}^0}}{\text{Tr } e^{-\beta \hat{h}_{iB}^0}} \tag{2.6}$$

where $\beta = 1/k_B T$, and we have again labeled the density operator by the number of vibrational modes in each PBI-1 molecule.

To formulate a physical picture of the EV dynamics, we investigate the time evolution of select electronic-vibrational densities (EVD). Specifically, we define the following intermolecular two-mode EVDs for the two electronic states of the dimer:

$$D_{iA,iB}^{1_A 0_B}(q_{iA}, q_{iB}; t) = \langle 1_A 0_B; q_{iA} q_{iB} | e^{-i\hat{H}_{\text{dimer}}^{1,1} t/\hbar} \hat{\rho}_{\text{dimer}}^{1,1}(0) e^{i\hat{H}_{\text{dimer}}^{1,1} t/\hbar} | 1_A 0_B; q_{iA} q_{iB}\rangle$$
$$D_{iA,iB}^{0_A 1_B}(q_{iA}, q_{iB}; t) = \langle 0_A 1_B; q_{iA} q_{iB} | e^{-i\hat{H}_{\text{dimer}}^{1,1} t/\hbar} \hat{\rho}_{\text{dimer}}^{1,1}(0) e^{i\hat{H}_{\text{dimer}}^{1,1} t/\hbar} | 0_A 1_B; q_{iA} q_{iB}\rangle \tag{2.7}$$

These functions are obtained from the dimer Hamiltonian where only mode i is included in each molecule. We also define the intermolecular, two-mode projections of the all-mode EVD for the two states of the dimer, which are obtained from the dynamics of the full Hamiltonian with $\nu_A = \nu_B = 28$ after tracing with respect to all modes besides i,

$$\bar{D}_{iA,iB}^{1_A 0_B}(q_{iA}, q_{iB}; t) = \text{Tr}_{i' \neq i} \langle 1_A 0_B; q_{iA} q_{iB} | e^{-i\hat{H}_{\text{dimer}}^{28,28} t/\hbar} \hat{\rho}_{\text{dimer}}^{28,28}(0) e^{i\hat{H}_{\text{dimer}}^{28,28} t/\hbar} | 1_A 0_B; q_{iA} q_{iB}\rangle$$
$$\bar{D}_{iA,iB}^{0_A 1_B}(q_{iA}, q_{iB}; t) = \text{Tr}_{i' \neq i} \langle 0_A 1_B; q_{iA} q_{iB} | e^{-i\hat{H}_{\text{dimer}}^{28,28} t/\hbar} \hat{\rho}_{\text{dimer}}^{28,28}(0) e^{i\hat{H}_{\text{dimer}}^{28,28} t/\hbar} | 0_A 1_B; q_{iA} q_{iB}\rangle \tag{2.8}$$

Further, we define the following intramolecular two-mode EVDs for the two states of the dimer, where modes i and j are included on monomer A,

$$D_{iA,jA}^{1_A 0_B}\left(q_{iA},q_{jA};t\right)=\left\langle 1_A 0_B;q_{iA}q_{jA}\left|e^{-i\hat{H}_{dimer}^{2,0}t/\hbar}\hat{\rho}_{dimer}^{2,0}\left(0\right)e^{i\hat{H}_{dimer}^{2,0}t/\hbar}\right|1_A 0_B;q_{iA}q_{jA}\right\rangle$$

$$D_{iA,jA}^{0_A 1_B}\left(q_{iA},q_{jA};t\right)=\left\langle 0_A 1_B;q_{iA}q_{jA}\left|e^{-i\hat{H}_{dimer}^{2,0}t/\hbar}\hat{\rho}_{dimer}^{2,0}\left(0\right)e^{i\hat{H}_{dimer}^{2,0}t/\hbar}\right|0_A 1_B;q_{iA}q_{jA}\right\rangle$$

(2.9)

as well as the intramolecular two-mode projection of the all-mode EVDs,

$$\tilde{D}_{iA,jA}^{1_A 0_B}\left(q_{iA},q_{jA};t\right)=\text{Tr}_{i'\neq i}\text{Tr}_{j'\neq j}\left\langle 1_A 0_B;q_{iA}q_{jA}\left|e^{-i\hat{H}_{dimer}^{28,28}t/\hbar}\hat{\rho}_{dimer}^{28,28}\left(0\right)e^{i\hat{H}_{dimer}^{28,28}t/\hbar}\right|1_A 0_B;q_{iA}q_{jA}\right\rangle$$

$$\tilde{D}_{iA,jA}^{0_A 1_B}\left(q_{iA},q_{jA};t\right)=\text{Tr}_{i'\neq i}\text{Tr}_{j'\neq j}\left\langle 0_A 1_B;q_{iA}q_{jA}\left|e^{-i\hat{H}_{dimer}^{28,28}t/\hbar}\hat{\rho}_{dimer}^{28,28}\left(0\right)e^{i\hat{H}_{dimer}^{28,28}t/\hbar}\right|0_A 1_B;q_{iA}q_{jA}\right\rangle$$

(2.10)

The projected EVDs describe the motion of the vibrational components associated with the specific modes on the $\left|1_A 0_B\right\rangle$ and $\left|0_A 1_B\right\rangle$ electronic states as a function of time, averaged with respect to all other vibrational degrees of freedom.

All calculations are performed through quadrature-based path integral methods, namely the quasi-adiabatic propagator path integral[16-19] (QuAPI), along with its small matrix decomposition[20-22] (SMatPI). These fully quantum mechanical methods allow us to include the finite-temperature dynamics of all vibrational modes in each molecular unit without approximation through analytically evaluated influence functional[23] factors. A summary of these methods as they pertain to the EV-RDM in these coupled chromophore arrays was given in another recent paper.[11] The reader is referred to the cited articles for detailed presentations of these theoretical tools.

III. Simple and general considerations governing EVD evolution in a homodimer

Consider first a single mode on each of the two molecules, with frequencies ω_{iA} and ω_{jB}. Figure 1 shows a pictorial description of the EV framework for the dimer. The two electronic states define a pair of two-dimensional diabatic potential energy surfaces (square frames) coupled by the Frenkel exciton coupling parameter J. As shown by the red contours, the potential minimum on the $\left|1_A 0_B\right\rangle$ surface (on the right) is shifted horizontally (along q_{iA}) from the origin to q_{iA}^{min}, while the corresponding shift along the vertical axis lies at $q_{iB}=0$. Similarly, the coordinates of the potential minimum on the $\left|0_A 1_B\right\rangle$ surface lie at $q_{iA}=0$, q_{jB}^{min}. At $t=0$ monomer A is excited, thus creating a Gaussian density (gray ellipse) on the $\left|1_A 0_B\right\rangle$ surface of widths determined by the two vibrational frequencies and the temperature. Because of the FC initial condition, the density is centered at the origin and displaced with respect to the potential minima by the amounts q_{iA}^{min} and q_{jB}^{min}.

At zero temperature the initial density is given by the square of the ground state wavefunction, which is a Gaussian function. If the two electronic surfaces are uncoupled and in the absence of other vibrational degrees of freedom, one-dimensional, fixed-amplitude harmonic wavepacket oscillations are observed on the $\left|1_A 0_B\right\rangle$ surface along q_{iA}, where the center of the wavepacket moves between the two classical turning points with coordinates 0 and $2q_{iA}^{min}$, with no loss in total density.[24] Conversely, if the exciton-vibration coupling $c_{i\alpha}$ is set to zero, energy transfer between the two states creates two-level system (TLS) oscillations with a time scale corresponding to the electronic energy gap. This case translates to a static Gaussian wavepacket, with periodically growing and diminishing height. When both J and $c_{i\alpha}$ are nonzero, along with the initial density motion to the right on the $\left|1_A 0_B\right\rangle$ surface, simultaneous state-to-state energy transfer leads to the gradual loss of density, creating a new wavepacket on the $\left|0_A 1_B\right\rangle$ surface (yellow ellipse). The Landau-Zener model[25-27] offers an insightful picture for the dependence of the nonadiabatic

transfer rate on the local potential slopes, strength of coupling and wavepacket velocity, but the overall motion is rather complex[28] even in the two-dimensional case considered here. Depending on the relative magnitudes of J and ω_{iA}, the peak of this new wavepacket lies somewhere between 0 and $2q_{iA}^{min}$ along the q_{iA} axis, thus creating displacements from the potential minimum of the $|0_A 1_B\rangle$ surface in both vertical and horizontal directions. Therefore, the wavepacket on the $|0_A 1_B\rangle$ state moves along both coordinates. As the density on this state grows while the initially excited state begins to be depleted, nonadiabatic back-transfer takes place, adding probability density to the $|1_A 0_B\rangle$ state at a different location (green ellipse), in the vicinity of the surface crossing region (the seam). This back-transfer leads to motion along both coordinates on this state as well, and creates the possibility of interference between the two spatially separated wavepackets, one diminishing and the other growing in intensity. This picture shows how the simultaneous electronic and exciton-vibration interactions lead to two-dimensional wavepacket dynamics on both electronic states. At nonzero temperatures the dynamics can be analyzed in similar ways, but the distinct spatial characteristics of excited vibrational wavefunctions lead to modified wavepacket dynamics and temperature-dependent EVD evolution.
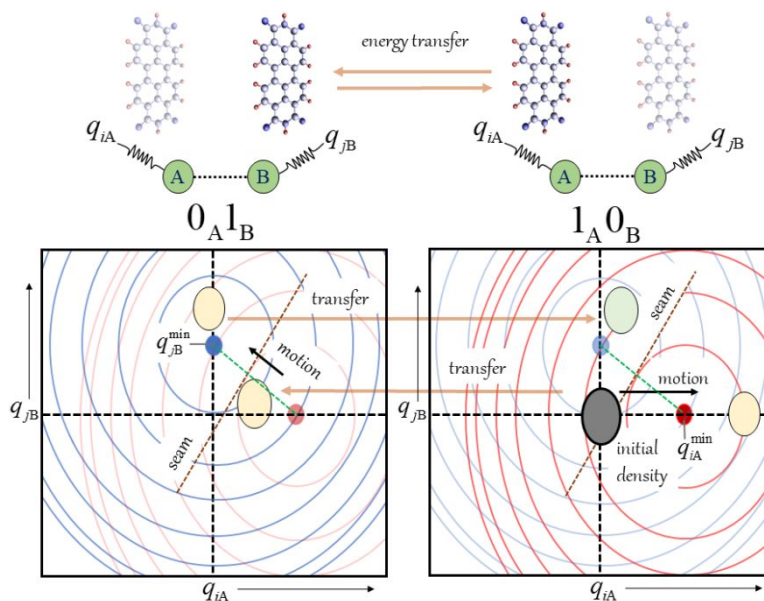

Fig. 1. Simple illustration of vibrational density motion on the two electronic surfaces with a single vibrational mode in each monomer.

Using the quantum-classical path integral formulation[29] of nonadiabatic dynamics, one can see that vibrational motion modifies the exciton transfer dynamics through a phase that depends on the local reorganization energy, i.e. the difference between the two diabatic potential values.[30] Fig. 1 shows the seam, i.e. the line of zero reorganization energy, which is tangent to the potential contours at the point of intersection with the line that connects the two potential minima. The slope of the seam is equal to c_{iA}/c_{jB}.

The reorganization energy is constant along lines parallel to the seam. As a result, motion in directions parallel to the seam does not modify the vibrational phase, thus should not produce EV effects. Note that in general the seam is not perpendicular to the line connecting the potential minima.

The picture simplifies if the two modes q_{iA} and q_{jB} have the same frequency and coupling coefficient ($j = i$), which implies identical displacements of potential minima and circular contours in Fig. 1. The frequency degeneracy implies that any linear combination of the coordinates maintains the separability of the diabatic potentials. It has been shown[31, 32] that only the difference linear combination $q_{iA} - q_{iB}$ couples to the pair of electronic states, while the sum coordinate combination is uncoupled and thus does not alter the EET dynamics, although the density moves along this coordinate as well. The coupled antisymmetric mode combination coincides with the line that connects the potential minima, while the sum coordinate is parallel to the seam line. These two lines are perpendicular in this case. Motion along the difference coordinate $q_{iA} - q_{iB}$ incurs the largest reorganization energy. We thus expect important strongly correlated EV dynamics along this direction.[33] On the other hand, motion parallel to the seam line does not change the vibrational energy, thus does not modify the rate of state-to-state transfer.
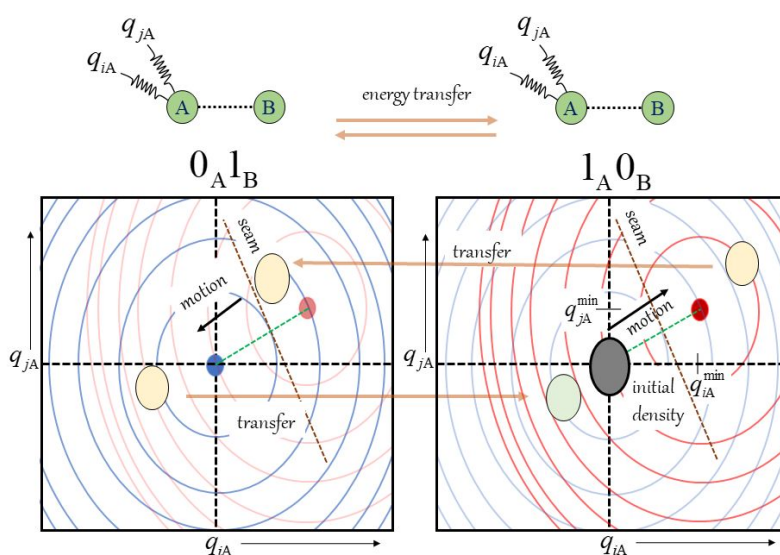

Fig. 2. Motion of vibrational densities on the two electronic surfaces for two different vibrational modes on the same molecule.

Next, we focus on the EV dynamics in the case of two distinct normal modes *i* and *j* of different frequencies that are coupled to the same molecule. Since both modes are now excited and de-excited simultaneously by EET, the arrangement of potential energy surfaces is modified and is shown in Figure 2. The minimum on the $|0_A1_B\rangle$ state is now unshifted (i.e. the potential is centered about the origin), while on the $|1_A0_B\rangle$ state it is shifted along both coordinates. Since the frequencies of the modes are different, the diabatic potentials have elliptical shapes and their minima are displaced by different amounts along the two modes. With $J = 0$ the motion at zero temperature is that of a two-dimensional Gaussian wavepacket,[24]

whose center executes Lissajous rotations[34] within a rectangular region specified by the two displacement values. In the presence of nonzero electronic coupling the two-dimensional motion leads to the creation of density (yellow ellipse) on the $|0_A 1_B\rangle$ state which is also displaced along both coordinates.

In the parameters of the two modes are identical, as in the case of two degenerate intramolecular normal modes, the motion simplifies again along the sum and difference linear combinations of the vibrational coordinates. In this case the difference coordinate is parallel to the seam and decouples from the electronic dynamics, while the symmetric mode $q_{iA} + q_{iB}$ couples to the electronic states and thus gives rise to EV effects. While the individual normal modes q_{iA} and q_{iB} are completely correlated, the wavefunction (and density) factorizes along the new sum and difference modes.

The specifics of both kinds of motion illustrated in Figures 1 and 2 are the outcome of the complex interplay of electronic and vibrational parameters as well as the temperature. Further, the projected densities, which result from the complex motion of many vibrational degrees of freedom, incorporate dephasing effects that mimic to some extent those in dissipative environments. The detailed dynamics of EET in the PBI-1 dimer are described in the next section.

IV. Evolution of electronic-vibrational densities in the PBI-1 dimer

The electronic coupling J in the PBI-1 dimer is $514\,\text{cm}^{-1}$, giving rise to an energy gap $2J = 1028\,\text{cm}^{-1}$, which defines the electronic period equal to $\tau_{\text{el}} = 32$ fs. The spectral density for the PBI-1 molecule,[15] depicted in Figure 3a, comprises 28 normal modes spread over a large range of vibrational frequencies (7-1628 cm^{-1}) with varying exciton-vibration coupling strengths. Mode q_{25}, with a frequency $q_{25} = 1371\,\text{cm}^{-1}$ (i.e. somewhat higher than the frequency of the electronic system), has the strongest coupling to the electronic states. Mode q_{27}, of a higher frequency, is also strongly coupled.
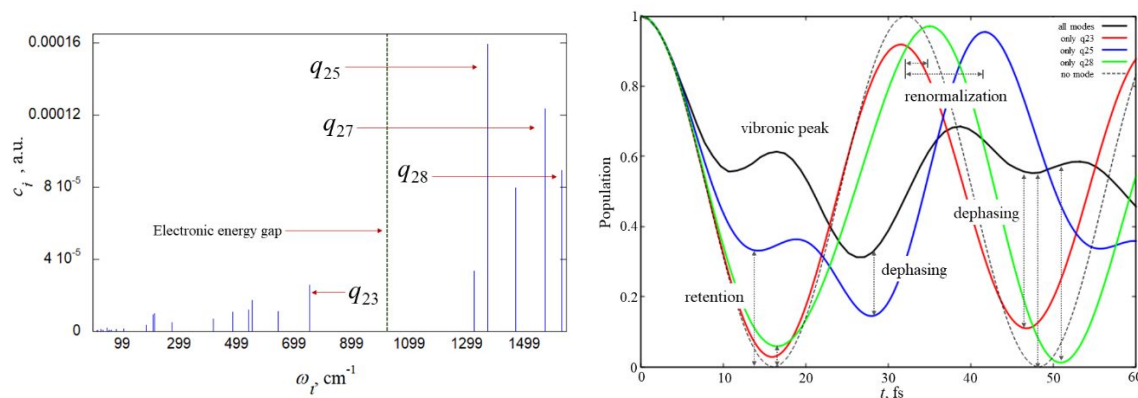

Fig. 3. (a) Spectral density of PBI-1 (from Ref. [15]). The vibrational modes whose EVD are analyzed are marked. The dashed line indicates the frequency associated with the electronic energy gap. (b) Population of initially excited state in the PBI-1 dimer, illustrating the main effects of exciton-vibration dynamics discussed in the text. Dashed black line: dynamics in the absence of vibrational modes. Red, blue and green lines: mode q_{23}, q_{25} and q_{28}, respectively, included in both molecules. Solid black line: all vibrational modes included.

Figure 3b shows the population of the $|1_A 0_B\rangle$ state in the absence of vibrations, with a particular vibrational mode included in each of the two molecules, and also with all modes included. Before presenting the detailed EVD evolution we give a brief overview of the main features of population dynamics along with their EV origins:

(i)   Amplitude reduction of population oscillations due to density retention. This feature arises from partial population retention along each normal mode coordinate when the density moves sufficiently far from the crossing region. The extent of retention ranges from negligible or minor in the weakly coupled modes with small diabatic potential displacements and is substantial in the case of the strongly coupled mode q_{25}.

(ii)   Damping of oscillatory features due to the collective decohering effects of many vibrational modes. This effect is the consequence of dephasing caused by the simultaneous presence of many vibrational modes with a significant frequency spread and is more pronounced at longer times and at higher temperatures.

The combination of effects *(i)* and *(ii)* is a smearing of electronic populations.

(iii) Renormalization of electronic energies by vibrational modes, leading to delayed recurrences of population. This effect is primarily due to the five highest frequency vibrations[12] and is analogous to the well-studied bath-induced renormalization of tunneling splittings.[35, 36]

(iv)   Emergence of new oscillatory features characterized by a very weak temperature dependence. These features are associated with a *vibronic* time scale faster than the purely electronic dynamics, although indirect coupling to many weakly coupled modes significantly influences such features.

We now illustrate these features by presenting the detailed EVD evolution in the PBI-1 dimer. We use the length parameter $\sqrt{h/m\omega_i}$, which equals half of the width of the classically accessible region for the harmonic oscillator ground state, to quantify the displacement of diabatic potential minima and the coordinates of turning points. We examine the features of EVD evolution for combinations of modes q_{23}, q_{25}, q_{27} and q_{28}. These modes are characterized by the following parameters:

$$q_{23}: \omega_{23} = 751 \text{ cm}^{-1}, q_{23}^{min} = 0.2569\sqrt{h/m\omega_{23}}$$
$$q_{25}: \omega_{25} = 1371 \text{ cm}^{-1}, q_{25}^{min} = 0.6449\sqrt{h/m\omega_{25}}$$
$$q_{27}: \omega_{27} = 1570 \text{ cm}^{-1}, q_{27}^{min} = 0.4074\sqrt{h/m\omega_{27}}$$
$$q_{28}: \omega_{28} = 1628 \text{ cm}^{-1}, q_{28}^{min} = 0.2792\sqrt{h/m\omega_{28}}$$

In Figures 4-6 we show ten representative frames in the 0-50 fs time window for each case. The detailed frame-by-frame motion can be seen in the animations available as Supporting Information to this paper.

A. EVD evolution with a single vibrational mode in each monomer

As depicted in Fig. 1, when both modes have identical parameters, the line that connects the two potential minima makes an angle equal to 135° with respect to the horizontal axis and is perpendicular to the seam. The two minima and the peak of the initial density form an isosceles right triangle.

In Figure 4 (left panel) we show the EVD evolution for mode q_{23} (attached to each monomer), which has a frequency $\omega_{23} = 751 \text{ cm}^{-1}$ (period $\tau_{23} = 44 \text{ fs}$) and thus is a relatively slow mode with a small displacement value $q_{23}^{min} = 0.2569\sqrt{h/m\omega_{23}}$. With these parameters the density on each potential surface remains primarily compact and Gaussian-like, although some elongation is observed in several frames.
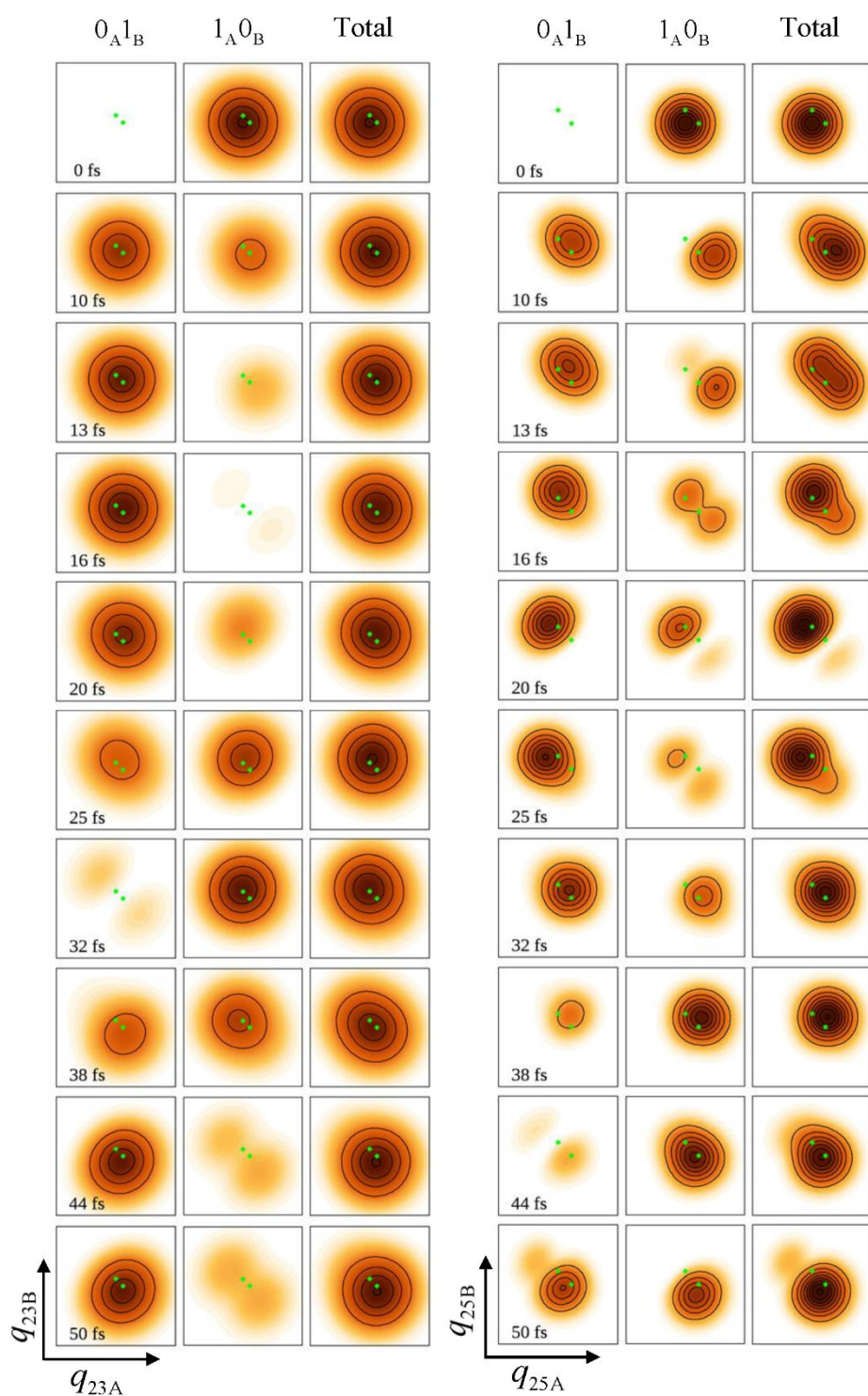
Fig. 4. EVD evolution on the two electronic states along the two q_{23} (left) and the two q_{25} (right) modes coupled to molecules A and B. The first and second column in each panel shows the EVDs on the $|1_A0_B\rangle$ and $|0_A1_B\rangle$ states, while the third column shows the total density. The green dots indicate the locations of the potential minima.

Further, since the distance between the minima of the two surfaces is much smaller than the spread of the density, the sum of the two densities also has the same compact shape.

As discussed earlier in the context of Figure 1, the density on the $|1_A 0_B\rangle$ state is initially displaced from the minimum and thus starts moving toward the right. The turning point, when the density is at its farthest beyond the potential minimum, would be reached at $\frac{1}{2}\tau_{23} = 22$ fs. However, because $\tau_{el} = 32$ fs, density is transferred from the $|1_A 0_B\rangle$ state to the $|0_A 1_B\rangle$ state (i.e. molecule A is de-excited and molecule B is excited) over the initial 16 fs. As a result, the innermost part of the density on the $|1_A 0_B\rangle$ diabatic surface is largely depleted before its peak reaches the turning point, leaving behind only a small fraction of the density that peaks around 16 fs, which resists electronic transfer because it is located far from the crossing region. This minor population retention is observed in the population dynamics of mode q_{23} shown in Fig. 3b.

The motion of the new density formed on the $|0_A 1_B\rangle$ surface is determined by two factors. Due to the displacement away from the minimum along q_{iB}, it encounters a upward force, while due to the motion of the surviving density on the $|1_A 0_B\rangle$ state to the right, new density is continuously added along q_{iA}. This gives the impression that the density travels toward the right. The combined effect of these two components is diagonal motion towards and past the crossing region, until the turning point is reached at 22 fs when we observe a reversal of direction. Meanwhile, electronic population is transferred back to the $|1_A 0_B\rangle$ state during the time period 16-32 fs, and minor density retention is now observed on the $|0_A 1_B\rangle$ surface. Interestingly, this new population that arrives in the $|1_A 0_B\rangle$ state starting at 16 fs is spatially separated from the gradually diminishing density that exists on the same state. This leads to a transient split density. Overall, for mode q_{23}, we observe relatively simple EVD evolution, with only minor smearing of the electronic peaks and transient low-amplitude split densities due to weak exciton-vibration interaction.

Next, we investigate the EVD frames for q_{25}, the strongest coupled mode in the spectral density with a vibrational frequency $\omega_{25} = 1371$ cm^{-1} ($\tau_{25} = 24$ fs). This is a high frequency mode with the strongest coupling and has a moderately large displacement $q_{25}^{min} = 0.6449\sqrt{h/m\omega_{25}}$, which leads to a large amount of vibrational energy. The higher frequency causes the initial motion to the right to be faster than density depletion due to transfer, while the large displacement takes the density farther away from the crossing region. As a result, we first observe a pronounced retention of EVD at 16 fs, which prevents the electronic population from falling to zero, as seen in Fig. 4b. The emerging EVD on the $|0_A 1_B\rangle$ state moves rapidly toward the potential minimum (i.e. left and upward), and the density that continues to emerge near the crossing region leads to an elongation along the line connecting the potential minima. After going through the outer turning point at 12 fs begins, this EVD begins to accelerate towards the crossing region. The high velocity of the density (a consequence of its large kinetic energy as it approaches the crossing region), combined with the mostly depleted $|1_A 0_B\rangle$ state, leads to the early back-transfer of population from the $|0_A 1_B\rangle$ to the $|1_A 0_B\rangle$ state beginning at 14 fs. Since the remaining density on the $|1_A 0_B\rangle$ state is still located far from the crossing region, a split, double-peaked EVD is observed on the $|1_A 0_B\rangle$ state between 13 and 25 fs.

A large displacement along the vibrational coordinate leads to considerable overlaps of the initial density with several (at least five in this specific case) vibronic eigenstates. Newer timescales are thereby introduced, some of which are faster than both the electronic and vibrational motions, causing premature transfer, which manifests itself as vibronic peaks in the population dynamics with a very weak temperature dependence.
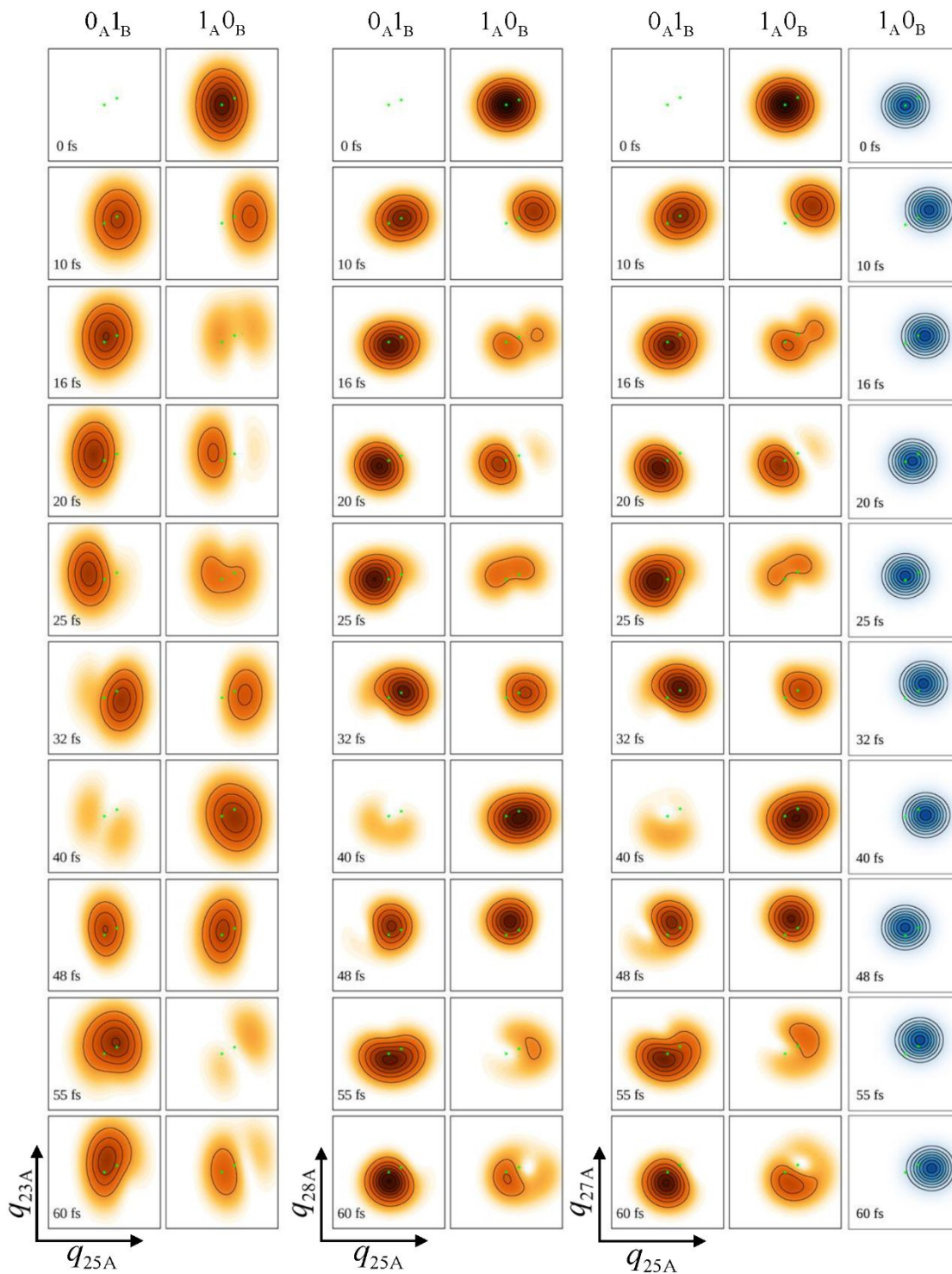
Fig. 5. EVD evolution along mode q_{25} (on the horizontal axis) and a second mode of molecule A. Left: q_{23} vs. q_{25}. Middle: q_{28} vs. q_{25}. Right: q_{27} vs. q_{25}. The time evolution of the density for $J = 0$ is shown with blue contours on the far right. The green dots indicate the locations of the potential minima.

The faster vibrational motion effectively slows down the transfer of electronic population between the two states. This occurs because the rapid motion of EVD away from the crossing region leads to depletion, which decreases the efficiency of population transfer. The resulting delay of electronic recurrence peaks is the dynamical manifestation of tunneling splitting renormalization[35, 36] whereby the energy difference between the two lowest electronic eigenstates is reduced due to coupling to a high frequency vibration.

As discussed in section III, the dimer Hamiltonian simplifies in the case where the same vibrational mode is coupled to each molecule, leading to a TLS coupled only to the difference coordinate. Thus the dimer Hamiltonian is separable in the sum and difference coordinates, implying factorization of wavefunctions and thus of the EVD as well. The consequence of this separability is evident in all the frames of Fig. 4. In particular, density retention, nodal lines and EVD elongation develop along the line connecting the potential minima, while only simple oscillatory motion is observed along the spectator coordinate parallel to the seam. We emphasize that the perfect correlation of these two vibrational modes is a symmetry effect, i.e. the manifestation of frequency degeneracy, and should be distinguished from effects due to indirect coupling among different normal modes discussed later.

B. EVD evolution with two vibrational modes in one monomer

The discussion in the previous subsection focused on the dynamics of two identical vibrational modes, one on each monomer, on the two electronic states of the dimer. Even though the density was a two-dimensional function, its evolution was governed by a single vibrational time scale. To explore the interplay of two vibrational time scales in the EET dynamics, along with the different geometrical features of the diabatic potentials with respect to the initial vibrational density, we present in Figure 5 the evolution of the EVD for two vibrational modes of the same molecule. As before, we show ten time frames and refer the reader to the animations available as Supporting Information for the full EVD dynamics on a 1 fs time grid. We present results for the following three pairs of normal modes: (i) q_{25} and q_{23}, (ii) q_{25} and q_{28}, and (iii) q_{25} and q_{27}.

Unlike in the previous case, the seam now makes an angle with the horizontal axis that exceeds 90°, while the line that connects the two potential minima makes an acute angle. Because the coordinate of mode q_{25} (which has the largest displacement) is placed on the horizontal axis, this angle is smaller than 45° in all cases. As described in the context of Fig. 2, the initial motion is primarily along this angled line, but because the two modes now reach their turning points at different times, Lissajous rotations[34] of the EVD are observed. In the absence of electronic coupling, the EVD maintains a fixed elliptical shape and its center undergoes Lissajous motion (see the rightmost panel of Figure 5), the trajectory of which depends on the ratio of the frequency of the two modes. However, when $J \neq 0$, state-to-state population transfer creates complex patterns, such as crescent-shaped densities and in some frames even internal holes in the density. These patterns carry information about how the dynamics of one vibrational mode is affected by other modes, to which it is coupled only indirectly.

The dynamics related to the vibronic features attributed to mode q_{25} (16-24 fs and 55-60 fs) is particularly interesting. Even though mode q_{25} is entirely responsible for the premature back-transfer of population that leads to the vibronic feature, Fig. 5 shows that the formed density is split along the angled line that connects the potential minima. This is so because the surviving EVD on the $|1_A 0_B\rangle$ state lies near or beyond the outer turning point in this two-dimensional space, while the back-transferred density emerges

close to the crossing region. Therefore, contrary to what one might expect, effectively the vibronic motion is not only along q_{25} but also along the weakly coupled non-vibronic mode.

Although the normal modes are not explicitly coupled in the Hamiltonian, their individual exciton-vibration interactions affect the motion of the EVB on the diabatic potential surfaces, which in turn determines the probability of nonadiabatic transfer at any given time. The complex interplay of these effects leads to behaviors that we describe as manifestations of indirect coupling among vibrational modes.

To obtain an alternative perspective and additional insights into the observed EVD evolution, we recall that since the parameters of the two modes are not identical, the EVD is not expected to be symmetric with respect to the line that connects the potential minima. Remnants of this symmetry can be discerned in Fig. 5, in particular in the case of modes q_{25} and q_{27} whose parameters differ less than those of the other pairs. Thus the shapes observed in Fig. 5 indicate two different types of indirect coupling to other modes: Departures from symmetry with respect to the 45° line indicate imperfect symmetry-induced mode correlation (i.e. the sum coordinate $q_{25} + q_{27}$ is not the only one coupled to the electronic states, but $q_{25} - q_{27}$ also contributes to the EV dynamics), while deviations from simple elliptical shapes suggest indirect mode-mode coupling enabled by the pair of electronic states.

C. EVD evolution in the presence of all vibrational modes

With an understanding of the EV effects caused by the simultaneous coupling to vibrational modes of different frequencies, we now proceed to analyze the full EVD dynamics etched with multiple vibrational time scales from all intramolecular vibrations. In Figure 6 we show the time evolution of the full EVD projected along the q_{23} or the q_{25} coordinate on both molecules. In both cases, the most prominent effect of the remaining vibrational modes is the smoothing of the density.

In the case of q_{23} there are five higher frequency modes in the spectral density with sufficiently large displacements. Therefore, we first note that the projected density in Fig. 6 shows considerable population retention on the $|1_A 0_B\rangle$ state, consistent with the similar effect observed in the electronic population. This is a cumulative effect of the population that remains not transferred during the first half of the electronic period along each of the 56 normal mode coordinates of the two molecules. Further, the vibronic feature of mode q_{25} also contributes to this projection along q_{23} as a peak in intensity, which in the presence of all the other modes occurs at 16 fs. Owing to both effects, we see a farther migration of the projected density away from the initially excited region along q_{23}, compared to the two-mode case. This suggests that the strongly coupled high-frequency vibrations cause this lower frequency mode to be effectively coupled more strongly to the electronic degree of freedom. Larger density displacements are also seen on the $|0_A 1_B\rangle$ state during the second half of the electronic period, now to the left of the minimum, which eventually lead to a delayed electronic recurrence.

In contrast to the effects on mode q_{23}, the same EVD projected onto the most strongly coupled mode q_{25} exhibits distinct features. Now the remaining modes are relatively weakly coupled, thus the resulting smoothing of the density is less pronounced. Interestingly however, the vibronic peak at 20 fs is now shifted to 16 fs in the presence of several other high-frequency modes of intermediate coupling strengths, in particular q_{26}, q_{27} and q_{28}, none of which alone have sufficiently strong exciton-vibration coupling to induce such vibronic features. This seemingly peculiar effect appears to be a manifestation of indirect coupling (through the electronic degree of freedom) among vibrational normal modes.
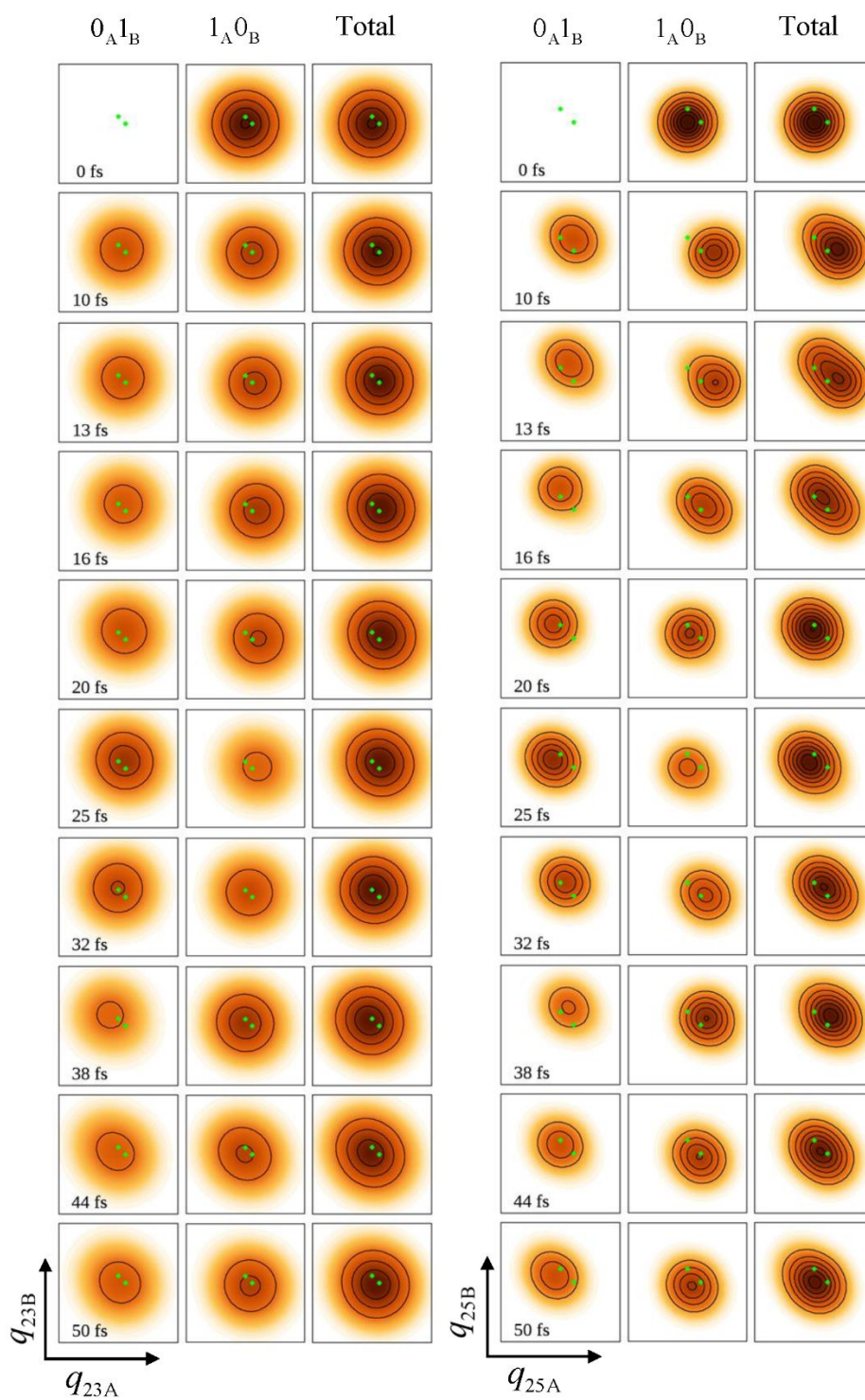
14

Fig. 6. Reduced same-mode, two-molecule EVD evolution on the two electronic states in the PBI-1 dimer. Left: mode q_{23}. Right: mode q_{25}. The three columns in each set show the densities on the states $|1_A 0_B\rangle$ and $|0_A 1_B\rangle$ and the total density. The green dots indicate the locations of the potential minima.

Nevertheless, due to the dephasing effects coming from other normal modes, the vibronic transfer no longer creates a split density. Rather, a continuous density is seen to go through a maximum at 16 fs. As before, the density reaches its turning points at 24 fs and 36 fs on the $\left|0_A 1_B\right\rangle$ state before showing a population transfer to the $\left|1_A 0_B\right\rangle$ state up to 40 fs. Effects of high frequency vibrational modes on the dynamics of low frequency modes were recently reported in an electron transfer reaction involving a PBI molecule as the donor.[37] Such inter-mode correlations, if strong enough, could lead to distinct vibrational signatures in EET and have important implications for inter-mode energy exchange.

V. Concluding Remarks

By examining the EVD evolution on electronic surfaces, we have presented a detailed mechanistic picture of EET in molecular aggregates. For a given vibrational initial state, the coupling between electronic and vibrational degrees of freedom, along with the vibrational frequencies, dictate the wavepacket motion on each electronic state, while the nonadiabatic coupling modifies this dynamics by adding or removing density. These two factors combine to give rise to highly nontrivial EVD dynamics, particularly in the case of strong exciton-vibration interaction. Thermal averaging further complicates the dynamics of the evolving density, as the spatial characteristics and temporal features associated with the wavepackets formed from different initial conditions do not coincide. Probability densities that split up, form crescents and even exhibit internal holes, were seen to frequently emerge through the complex interplay of electronic and vibrational time scales that form the backbone of EET processes.

Using the parameters of the PBI-1 dimer, we have shown how the simultaneous presence of identical or distinct vibrational modes shape the different dynamical trends of energy transfer. We have identified EV signatures in the electronic population dynamics for specific normal modes that lie in different parameter regimes. Coupling to vibrations was seen to cause retention of population due to motion away from the crossing region of electronic surfaces. Similarly, strong coupling to faster vibrational modes slows down energy transfer due to tunneling renormalization, which manifests itself as repeated and cumulative density retention that leads to a slower return of population to the initially excited state. In a particular case, we showed how strong coupling also leads to premature transfer of vibronic origin due to an elongation of the probability density around the crossing region. We argued that while the motion of the density involves all vibrational coordinates, strong EV effects arise from the motion perpendicular to the seam, during which the vibrational reorganization energy is maximized. The dephasing effect of a multitude of non-commensurate vibrational timescales on one mode was quantified by investigating the evolution of projected densities.

Overall, separable vibrational modes were found to be indirectly coupled due to their interactions with the common electronic degrees of freedom. When identical modes exist within the same or in neighboring molecules, the two modes are maximally correlated by symmetry. In this case the correlated mode is perpendicular to the seam between the diabatic potentials, thus all EV effects, such as density splitting and retention, take place along this coordinate. In the absence of such symmetries, i.e. when the parameters or two modes differ, the degree of this correlation depends on the promixity of the mode frequencies. Depending on the relation between parameters, indirect mode correlation effects can be characterized as deviations from Gaussian-like EVD shapes, or departures from factorizable EVD evolution along the line that connects the diabatic potential minima. Moreover, symmetry-induced correlations

efficiently modulate the electronic population dynamics by driving the EET in the direction perpendicular to the potential seam, where EV phase effects are most prominent. Therefore, indirect mode coupling and its related signatures are fundamental to EET processes.

On the short-to-intermediate time interval for which results were presented, the smearing induced by the intramolecular vibrations of the two molecules resembles dissipative effects on the dynamics of the one or two tagged modes. Clearly, the finite-dimensional normal mode baths of the PBI dimer cannot generate true dissipative dynamics at long times. The addition of a dissipative bath to an EV Hamiltonian leads to further smoothing of the EVD, which eventually evolves toward an equilibrium distribution. [38] Further, even though we observed indirect coupling of different normal modes through their interaction with the electronic degree of freedom, our Hamiltonian did not include anharmonic potential terms, which would introduce direct mode coupling to the dynamics on each diabatic potential, along with the intricate signatures of nonlinear dynamics frequently observed in intramolecular vibrational energy redistribution.

In conclusion, we believe that the EVD effects that were delineated in this paper are sufficiently general enough to help in forming an intuitive picture of EET in terms of EV probability density dynamics. Besides facilitating the rationalization of theoretical and experimental results, the behaviors revealed through these calculations will aid in the quest for the design of materials with targeted function.

Conflicts of Interest

There are no conflicts to declare.

References

1. V. May and O. Kühn, *Charge and energy transfer dynamics in molecular systems*, Wiley, 3rd edn., 2011.
2. T. Mancal, J. Dostal, J. Psencik and D. Zigmantas, *Canadian Journal of Chemistry*, 2014, **92**, 135-143.
3. M. Schröter, S. D. Ivanov, J. Schulze, S. P. Polyutov, Y. Yan, T. Pullerits and O. Kühn, *Physics Reports*, 2015, **567**, 1-78.
4. A. Chenu and G. D. Scholes, *Annual Review of Physical Chemistry*, 2015, **66**, 69-96.
5. J. Cao, R. J. Cogdell, D. F. Coker, H.-G. Duan, J. Hauer, U. Kleinekathöfer, T. L. C. Jansen, T. Mančal, R. J. D. Miller, J. P. Ogilvie, V. I. Prokhorenko, T. Renger, H.-S. Tan, R. Tempelaar, M. Thorwart, E. Thyrhaug, S. Westenhoff and D. Zigmantas, *Science Advances*, 2020, **6**, eaaz4888.
6. X.-Q. Li, X. Zhang, S. Ghosh and F. Würthner, *Chemistry − A European Journal*, 2008, **14**, 8074-8078.

7.   F. Würthner, C. R. Saha-Möller, B. Fimmel, S. Ogi, P. Leowanawat and D. Schmidt, *Chemical Reviews*, 2016, **116**, 962-1052.
8.   F. Würthner, C. Thalacker, S. Diele and C. Tschierske, *Chemistry – A European Journal*, 2001, **7**, 2245-2253.
9.   T. E. Kaiser, H. Wang, V. Stepanenko and F. Würthner, *Angewandte Chemie International Edition*, 2007, **46**, 5541-5544.
10.   F. Würthner, T. E. Kaiser and C. R. Saha-Möller, *Angew. Chem. Int. Ed.*, 2011, **50**, 3376-3410.
11.   S. Kundu and N. Makri, *J. Phys. Chem. C*, 2021, **125**, 201-210.
12.   S. Kundu and N. Makri, *J. Chem. Phys.*, 2021, 114301.
13.   J. Frenkel, *Phys. Rev.*, 1931, **37**, 17.
14.   K. Huang and A. Rhys, *Proceedings of the Royal Society of London. Series A. Mathematical and Physical Sciences*, 1950, **204**.
15.   D. Ambrosek, A. Köhn, J. Schulze and O. Kühn, *The Journal of Physical Chemistry A*, 2012, **116**, 11451-11458.
16.   N. Makri, *Chem. Phys. Lett.*, 1992, **193**, 435-444.
17.   M. Topaler and N. Makri, *Chem. Phys. Lett.*, 1993, **210**, 448.
18.   N. Makri and D. E. Makarov, *J. Chem. Phys.*, 1995, **102**, 4600-4610.
19.   N. Makri and D. E. Makarov, *J. Chem. Phys.*, 1995, **102**, 4611-4618.
20.   N. Makri, *J. Chem. Phys.*, 2020, **152**, 041104.
21.   N. Makri, *Journal of Chemical Theory and Computation*, 2020, **16**, 4038–4049.
22.   N. Makri, *J. Chem. Theory and Comput. *, 2021, **17**, 1-6.
23.   R. P. Feynman and J. F. L. Vernon, *Ann. Phys.*, 1963, **24**, 118-173.
24.   E. J. Heller, *J. Chem. Phys.*, 1975, **62**, 1544-1555.
25.   L. D. Landau, *Z. Sowjun.*, 1932, **2**, 46.
26.   C. Zener, *Proc. R. Soc. A*, 1932, **137**, 696-703.
27.   E. Stueckelberg, *Helv. Phys. Acta*, 1932, **5**, 369.
28.   J. C. Tully, *The Journal of Chemical Physics*, 2012, **137**, 22A301.
29.   R. Lambert and N. Makri, *J. Chem. Phys.*, 2012, **137**, 22A553.
30.   N. Makri, *International Journal of Quantum Chemistry*, 2015, **115**, 1209-1214.
31.   S. B. Piepho, E. R. Krausz and P. N. Schatz, *Journal of the American Chemical Society*, 1978, **100**, 2996-3005.
32.   A. Bose and N. Makri, *J. Phys. Chem.*, 2020, **124**, 5028-5038.
33.   V. Tiwari, W. K. Peters and D. M. Jonas, *J. Chem. Phys.*, 2017, **147**, 154308.
34.   A. Lichtenberg and M. Lieberman, *Regular and chaotic dynamics*, Springer, 2nd edn., 1992.
35.   R. Silbey and R. A. Harris, *J. Chem. Phys.*, 1983, **80**, 2615-2617.
36.   A. J. Leggett, S. Chakravarty, A. T. Dorsey, M. P. A. Fisher, A. Garg and M. Zwerger, *Rev. Mod. Phys.*, 1987, **59**, 1-85.
37.   S. Rafiq, B. Fu, B. Kudisch and G. D. Scholes, *Nature Chemistry*, 2021, **13**, 70-76.
38.   S. Kundu and N. Makri, *J. Phys. Chem. B*, 2021, **in press**.